

# Atmospheric structure and dynamics of evolved massive stars. Thanks to 3D radiative hydrodynamical simulations of stellar convection

A. Chiavassa<sup>1,2</sup> 

<sup>1</sup>Université Côte d'Azur, Observatoire de la Côte d'Azur, CNRS, Lagrange, CS 34229, Nice, France

email: [andrea.chiavassa@oca.eu](mailto:andrea.chiavassa@oca.eu)

<sup>2</sup>Max-Planck-Institut für Astrophysik, Karl-Schwarzschild-Straße 1, 85741 Garching, Germany

## Abstract.

Evolved massive stars are major cosmic engines, providing strong mechanical and radiative feedback on their host environment. They contribute to the enrichment of their environment through a strong stellar winds, still poorly understood. Wind physics across the life cycle of these stars is the key ingredient to accomplish a complete understanding of their evolution in the near and distant Universe. Nowadays, the development of the observational instruments is so advanced that the observations became very sensitive to the details of the stellar surface making possible to quantitatively study what happens on their surfaces and above where the stellar winds become dominant. Three-dimensional radiative hydrodynamics simulations of evolved stars are essential to a proper and quantitative analysis of these observations. This work presents how these simulations have been (and will be) crucial to prepare and interpret a multitude of observations and how they are important to achieve the knowledge of the mass-loss mechanism.

**Keywords.** Massive evolved stars, hydrodynamics, radiative transfer

---

## 1. Introduction

Evolved and massive cool stars are major cosmic engines, providing strong mechanical and radiative feedback on their host environment (Langer 2012). Through strong stellar winds and supernova ejections, they enrich the interstellar medium with chemical elements, which are the building blocks for the next generation of stars. In particular, these objects are known to propel strong winds and stellar evolution models are not able to reproduce these winds without ad hoc physics. Therefore, a complete understanding of stellar evolution in the near and distant Universe and its impact on the cosmic environment cannot be achieved without a detailed knowledge of wind physics. This requires to trace the total mass ejected as well as its nature, the velocity of the winds, and the behaviour of the circumstellar envelope.

Massive ( $M \geq 8 M_{\odot}$ , the exact value of the upper limit depends on the treatment of convection; Höfner & Olofsson 2018) evolved cool stars are objects that have reached the late phases of their evolution when the nuclear fuel in the interior is almost exhausted. These stars grow dramatically in size and become Red Supergiant (RSG) stars. RSGs are precursors of core-collapse supernovae and bear high luminosity ( $L > 1000 L_{\odot}$ ) with effective temperatures between 3450 and 4100 K and stellar radii up to several hundreds

of  $R_{\odot}$ , or even more than  $1000 R_{\odot}$  (Levesque et al. 2005). Several mechanisms triggering mass-loss have been discussed, including magneto-hydrodynamic waves (Cranmer & Saar, 2011) and radiation pressure on molecules and dust (Josselin & Plez 2007), but still there is no realistic quantitative wind model (Meynet et al. 2015) that can explain the observed broad mass-loss rate range ( $\dot{M} = 10^{-7} - 10^{-4} M_{\odot}/\text{yr}$ ; De Beck et al. 2010). A whole picture of all the physical processes that simultaneously trigger and shape the strong winds is still missing. As underlined in Höfner & Olofsson (2018) and Decin (2021), the mass-loss mechanism is hard to discern because it involves a range of interacting, time-dependent physical processes on microscopic and macroscopic scales coupled with dynamical phenomena such as convection and pulsation in sub-photospheric layers, strong radiating shocks in the atmosphere, and dust condensation as well as radiative acceleration in the wind forming regions. In addition to this, it should also be noted that the situation is even more complex in the presence of (sub)stellar companions that are known to shape the outflow of cool evolved stars (Decin et al. 2020).

In this context, two physical processes play an important role in initiating and feeding up the strong mass-loss. In the first place the evolution of these objects is impacted by stellar convection. The convection process is non-local, three dimensional, and involves non-linear interactions over many disparate scale lengths. Moreover, it is often responsible for transporting heat up to the visible surface (Nordlund et al. 2009). In RSG atmospheres, convection is inferred from a few giant structures observed at the stellar surface with sizes comparable to the stellar radius and evolving on weekly or yearly time scales (Montargès et al. 2021, 2018; Chiavassa et al. 2010a, 2011a). These result into more extreme atmospheric conditions than in the Sun: very large variations in velocity, density and temperature produce strong radiative shocks in their extended atmosphere that can cause the gas to levitate and thus contribute to mass-loss (Höfner & Freytag 2019; Freytag et al. 2017; Chiavassa et al. 2011b).

The second ingredient is the magnetic field. Cranmer & Saar, (2011) presented a predictive description of mass-loss, based on Alfvén-wave-driven wind that require open flux tubes, radially directed away from the star, in order for the gas to be accelerated and escape (Höfner & Olofsson 2018). Several authors have detected and monitored over years low intensity integrated magnetic field of the order of 1-10 Gauss (Mathias et al. 2018; Aurière et al. 2010), but its origin is still under debate and it would most likely be very different from the dynamo at work in solar-type stars due to both their slow rotation and the fact that only a few convection cells are present at their surface at any given time (Aurière et al. 2010; Freytag et al. 2002).

## 2. 3D radiation-hydrodynamics simulations of stellar convection of massive evolved stars

In recent years, with increased computational power, it has been possible to compute grid of 3D radiation-hydrodynamics (RHD) simulations of the whole stellar envelope that are used to predict reliable synthetic spectra and images for several stellar types. The red supergiant star simulations are computed with CO5BOLD (Freytag et al. 2012). The code solves the coupled equations of compressible hydrodynamics and non-local radiative energy transport in the presence of a fixed external spherically symmetric gravitational field on a 3D cartesian grid. No artificially pulsations are added to the simulations (e.g., by a piston) but they are self-excited. The code uses a *óstar-in-a-boxó* configuration where the computational domain is a cubic grid equidistant in all directions; the same open boundary condition is employed for all sides of the box. The 3D simulations are characterized by realistic input physics and reproduce the effects of convection and non-radial waves. Currently they do not include a radiative-driven wind. The important input parameters for the simulation are (Chiavassa et al. 2011b): the stellar mass (contributing

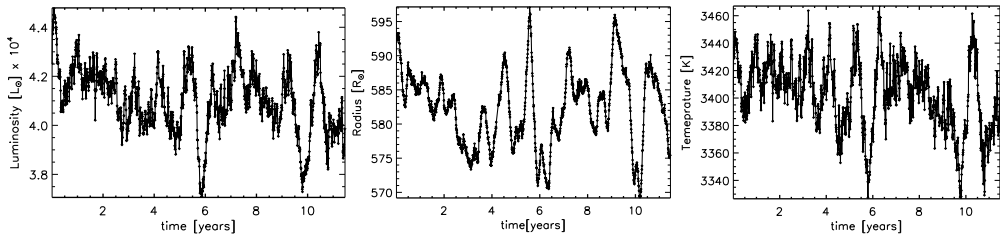


**Figure 1.** Spherical averages of the luminosity (left), the radius (center), and the effective temperature (right) as a function of time. See Table 1 for more details.

**Table 1.** Stellar parameters of the RHD simulation used in this work. The first column shows the simulation name, then the next 5 columns the stellar parameters such as the total mass, the average luminosity, the radius, the effective temperature, and the surface gravity. The different quantities are averaged over spherical shells (as in Chiavassa et al. 2009) and epochs (7th column,  $t_{\text{avg}}$ ). Errors are one standard-deviation fluctuations with respect to the time average. The solar metallicity is assumed.

Simulation	$M_*$ [ $M_\odot$ ]	$L_*$ [ $L_\odot$ ]	$R_*$ [ $R_\odot$ ]	$T_{\text{eff}}$ [K]	$\log g$ [cgs]	$t_{\text{avg}}$ [yr]	Grid points	$x_{\text{box}}$ [ $R_\odot$ ]
st35gm04n38	5	41517.3±1074.4	582.03±4.7	3414.2±16.8	-0.40±0.01	11.46	401 <sup>3</sup>	1631

to the gravitational potential), the input luminosity in the core, and the abundances that were used to construct the equation-of-state and the opacity tables. The latter are gray or use a frequency-binning scheme (3 to 5 bins). In the end, average values of stellar radius, effective temperature, and surface gravity have to be derived from a relaxed model (Fig. 1). Once the RHD simulation is done, the snapshots are used for detailed post-processing treatment to extract interferometric, spectrophotometric, astrometric, and imaging observables that in the end are compared to the observations. For this purpose, we use the 3D pure-LTE radiative transfer code Optim3D (Chiavassa et al. 2009) to compute synthetic spectra and intensity maps. Optim3D takes into account the Doppler shifts caused by the convective motions. The radiative transfer is calculated using pre-tabulated extinction coefficients generated with the MARCS code (Gustafsson et al. 2008) and by adopting the solar composition of, e.g., Asplund et al. (2009).

### 3. What 3D simulations predict

In this Section, we show different properties of convection-related structures using a particular 3D RHD simulation. Table 1 display the temporal and spherical averaged stellar parameters and the numerical box details of this simulation, that has been compared to interferometric (Climent et al. 2020) and spectroscopic observations (Kravchenko et al. 2019). Fig. 1 shows that even if the simulation has reached a stable state, the spherical averaged quantities still varies as a function of time as a consequence of the turbulent medium. In the end, RHD simulations of massive evolved stars show a very heterogeneous photospheric pattern evolving on timescales of weeks to years (Chiavassa et al. 2011a). In the simulations, the radiation is of primary importance for many aspects of convection and the envelope structure in a RSG simulations. It does cool the surface to provide a somewhat unsharp outer boundary for the convective heat transport and it also contributes significantly to the energy transport in the interior. Below the photospheric visible layers (i.e., optical depth  $\tau_{\text{Rosseland}} > 1$ , the opacity has its peak causing a very steep temperature jump which is very prominent on top of upflow regions. At the same time a density inversion appears, which is a sufficient condition of convective instability (Chiavassa et al. 2011b).

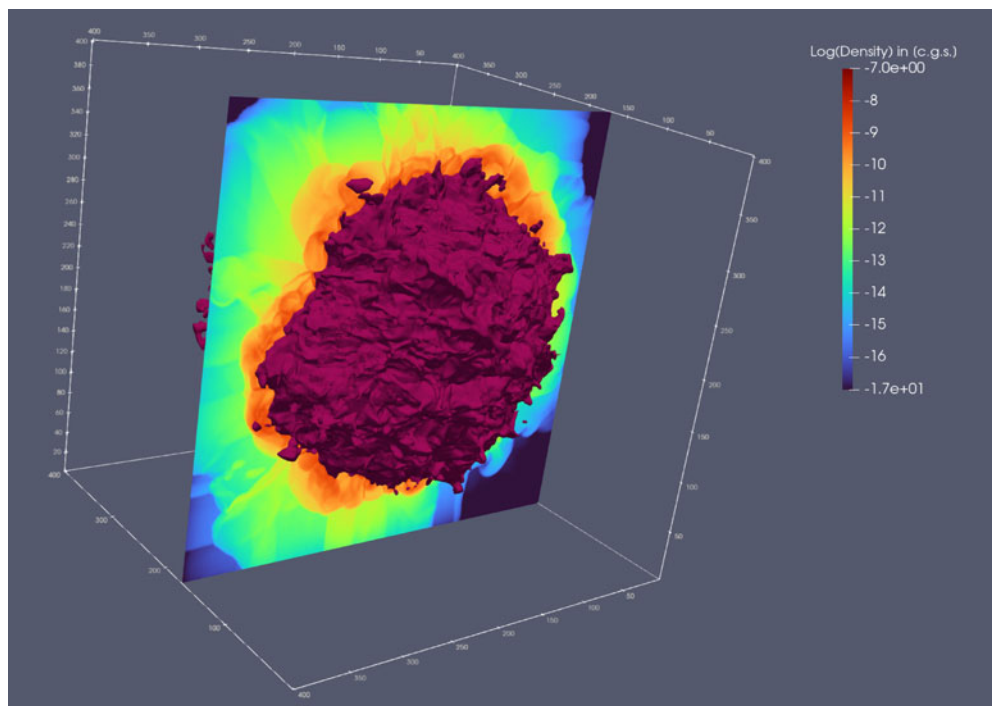


**Figure 2.** Logarithm of the density (from red to dark blue) of the 3D RHD simulation of Table 1 overlapped to the isosurface (amaranth color) of the Rosseland optical depth equal to one, where approximatively the continuum flux is formed.

The rising material originates in the deep convective zone (defined as the region below the Rosseland radius) and develops as an atmospheric shock when it reaches higher values in radius. This is explained in Freytag et al. (2017) and Liljegren et al. (2018): the sound waves produced by non-stationary convection (e.g., merging down-drafts or other localized events) travel through the stellar interior ( $\tau_{\text{Rosselend}} > 1$ ) to the outer layers ( $\tau_{\text{Rosselend}} \ll 1$ ) where the waves are slowed down and compressed because of the temperature drop. Moreover, in the outer layers (i.e., above the Rosseland radius) the density drops several orders of magnitude (Fig. 2) and the turbulent pressure dominates over the gas pressure ( $P_{\text{turbulent}}/P_{\text{gas}}$  is larger than 10, Chiavassa et al. 2011b) increasing the amplitude of the rising sound wave.

Eventually, the wave becomes a shock which propagates all the way from the stellar surface to the outer atmospheric layers with significant Mach numbers (up to 8, or even larger, Fig. 3). In these layers, the density (and the temperature) shows irregular structures with convection cells in the interior and a network of shocks in the atmosphere (Fig. 2). Local fluctuations in high Mach numbers and small-scale heights due to shocks pose high demands on the stability for the hydrodynamics. A side effect of the steep and significant temperature jump is the increase in pressure scale height from small photospheric values to values that are a considerable fraction of the radius in layers just below the photosphere.

Figure 4 displays the maps of the radial velocities. The fluffy layers (dark red, 20 km/s) correspond to the continuum forming region at Rosseland optical depth equal to one. Above, the high and heterogeneous velocities (up to  $\sim 30$  km/s) are accompanied by energetic pressure fluctuations, which in turn have a strong influence on shock waves. Following Freytag et al. (2017), who did this analysis for Asymptotic Giant Branch

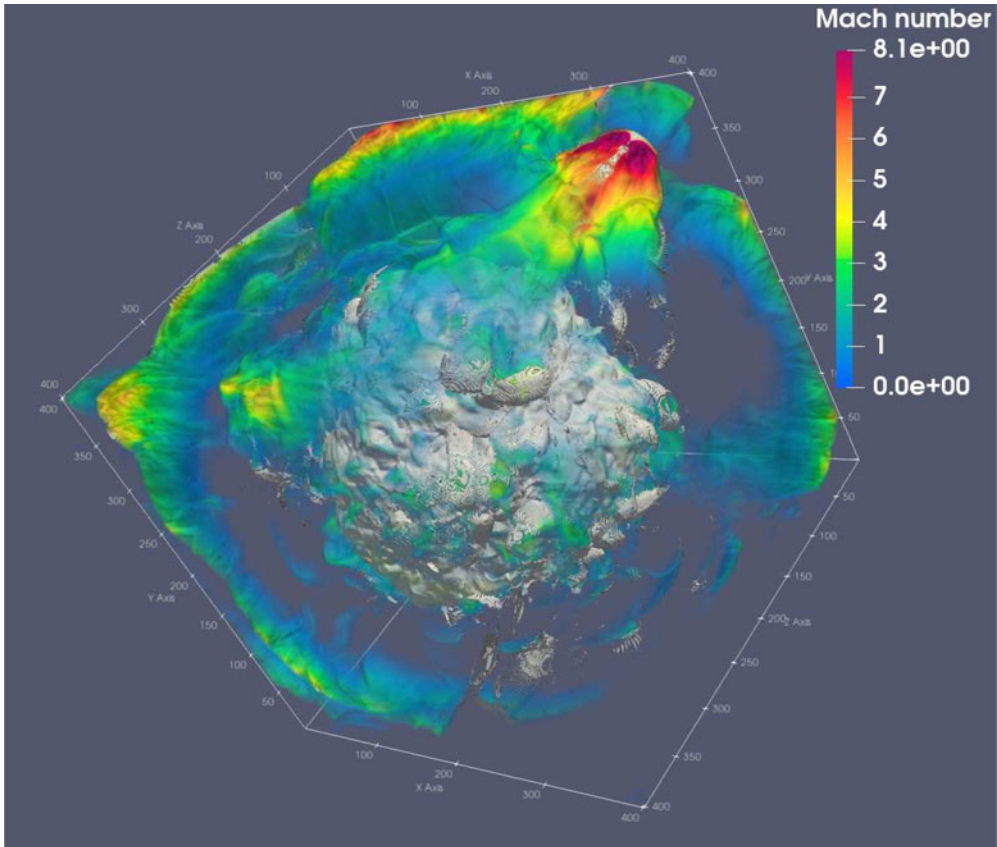


**Figure 3.** Radial Mach numbers computed for the 3D RHD simulation of Table 1 (blue to red colors) overlotted to the isosurface of the temperature equal to 3500 K (white). This temperature corresponds approximatively to the expected effective temperature of 3D simulations (Table 1). The simulations shows that the outer boundaries are either hit at some angle by an outgoing shock wave or let material fall back (mostly with supersonic velocities larger than Mach  $\sim 3$ , Fig. 4). In the end, the shocks pass through the boundaries with a simple and stable prescription in the code based on filling typically two layers of ghost cells where the velocity components and the internal energy are kept constant Freytag et al. (2012).

(AGB) simulations, we investigated the radial motions in the photosphere using averages over spherical shells of the radial velocities for each snapshot (Fig. 5). As for AGB stars, the behavior of the inner part of the model differs from that of the outer layers: below  $\sim 600 R_{\odot}$  (the nominal radius is  $582 R_{\odot}$ , Table 1) the velocity field is rather regular and coherent over all layers, close to a standing wave. The different slopes visible in the outer layers (above  $\sim 600 R_{\odot}$ ) are clearly indicating the presence of propagating shock waves but in a much less regular and smooth way than in the AGB case (as a matter of comparison, see Fig. 5 of Freytag et al. 2017).

#### 4. Two examples of applications for 3D simulations: convection cycles and spatially resolved surfaces

To provide quantitative constraints to the physics of massive evolved stars, observational techniques have reached such a level of excellence that it is now possible to reconstruct spatially and temporal resolved images of the stellar surface in the near IR and in the optical with interferometric or imagery techniques (e.g., Montargès et al.

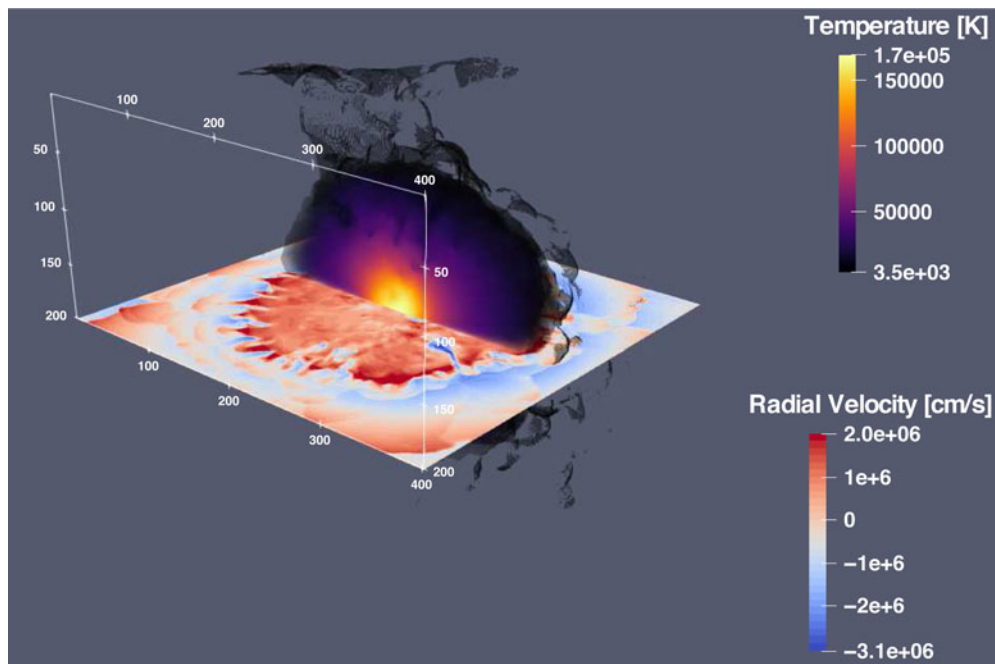


**Figure 4.** Central slice across the box of Fig. 3 showing the radial velocity: blue indicates outward and red inward flow. In addition to the velocities, the temperature volume rendering is also displayed (yellow to black colors). The temperature values arbitrary stops at 3500 K to show the approximative position of the  $\tau_{\text{Rosselend}} = 1$ , while in the simulation the temperature range covered is between  $\sim 1000$  and  $170\,000$  K. The large shocks can be up to  $\sim 250 R_{\odot}$  wide (each grid point is about  $4 R_{\odot}$ ) with local temperature of  $\sim 2500$  K and  $\log(\text{density in [c.g.s.]})$  of  $\sim -13$ .

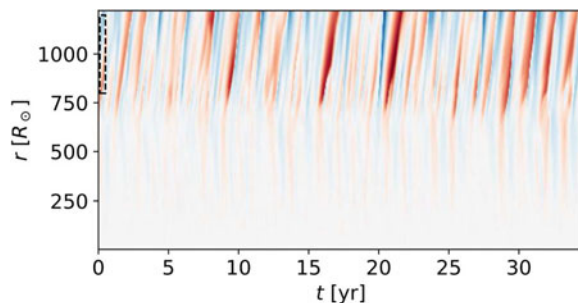


**Figure 5.** Spherically averaged radial velocities for the full run time and radial distance of the simulation of Table 1. The different colors show the average vertical velocity at that time and radial distance. The velocity range and color is the same as in Fig. 4.

2021; Norris et al. 2021; Cannon et al. 2021; Climent et al. 2020; Montargès et al. 2018; Ohnaka et al. 2017; Kervella et al. 2016; Chiavassa et al. 2010b; Haubois et al. 2009). In addition to this, long term spectro-photometric surveys are also available for observing RSG stars (e.g., Kravchenko et al. 2021, 2019; Lebzelter et al. 2019; Mathias et al. 2018; Kiss et al. 2006). The interpretation of these observations requires realistic modelling that takes into account most of the processes at work in the atmosphere (i.e., convection, shocks, pulsation, radiative transfer, ionization, molecules and dust formation, magnetic field). We present in this Section two examples based on the 3D RHD simulations done with CO5BOLD code and post-processed with the radiative transfer code Optim3D.

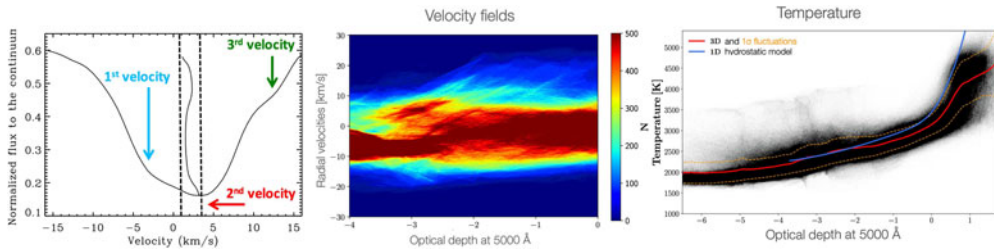


**Figure 6.** *Left panel:* Synthetic spectral line of the Ti I at 6261.11 Å for one snapshot of a 3D RHD simulation of an RSG star (Chiavassa & Freytag 2015). The vertical dashed line shows the spanned velocities of the line bisector. The different arrows and colors display the positions of different velocity components which contribute to the shape of the line. *Central panel:* The distribution of vertical velocities extracted from a 3D simulation as a function of the optical depth at 5000 Å. The color code shows areas with high (red) or low (blue) density of points (Kravchenko et al. 2018). *Right panel:* 3D simulation of the thermal structure. Darker areas correspond to more frequent temperature values. The red line is the mean 3D temperature profile. The orange dashed lines correspond to the one  $\sigma$  values around the average. The blue line refers to a 1D hydrostatic model.

#### 4.1. Convection cycles

RHD simulations provide a self-consistent ab-initio description of the non-thermal velocity field generated by convection, shock waves, and overshoot that manifests itself in spectral line shifts and changes in the equivalent width. They combine important properties such as velocity amplitudes and velocity-intensity correlations, which affect the line shape, shift, and asymmetries. Figure 6 (left panel) shows an example for the optical Ti I line at 6261.11 Å. The line shape constitutes of more than one velocity component that contributes through the different atmospheric layers where the line forms. As a consequence, the line bisector<sup>†</sup> is not straight and span values up to 5 km/s on a temporal scale of few weeks (as already pointed out by Gray 2008). As the vigorous convection is prominent in the emerging flux, the radial velocity measurements for evolved stars are very complex and need a sufficiently high spectral resolution to possibly disentangle all the sources of macro-turbulence. In addition to the velocity field (Fig. 6, central panel), other elements affect the line formation: (i) the strength of the transition depends on the mean thermal gradient in the outer layers ( $\tau_{5000} < 1$  in right panel of Fig. 6), for instance a shallow mean thermal gradient weakens the contrast between the continuum and line forming regions; (ii) the temperature (and density) inhomogeneities that affect the opacity run through the photospheric layers where the line forms.

In this context, we used the tomographic method to recover the distribution of the component of the velocity field projected on the line of sight at different optical depths in the stellar atmosphere (Fig. 6, central panel). This method was proposed for the first time by Alvarez et al. (2000), Alvarez et al. (2001a), Alvarez et al. (2001b) for AGB stars and then adapted and implemented in Optim3D for RSGs by Kravchenko et al. (2018). The authors successfully managed to show that in 3D simulations, the spectral lines do not form in the same limited number of layers as in 1D hydrostatic models, but they spread over different optical depths due to the non-radial convective movements. Additionally, this method allows to recover the dependence of the velocity field across the atmosphere.

The tomography of the stellar photosphere tomographic opens a new doorway for the study of stellar dynamical cycles in evolved stars, and in particular RSGs.

<sup>†</sup> It is the locus of the midpoints of the line. A symmetric profile has a straight vertical bisector, while the "C"-shaped line bisector reveals asymmetries.

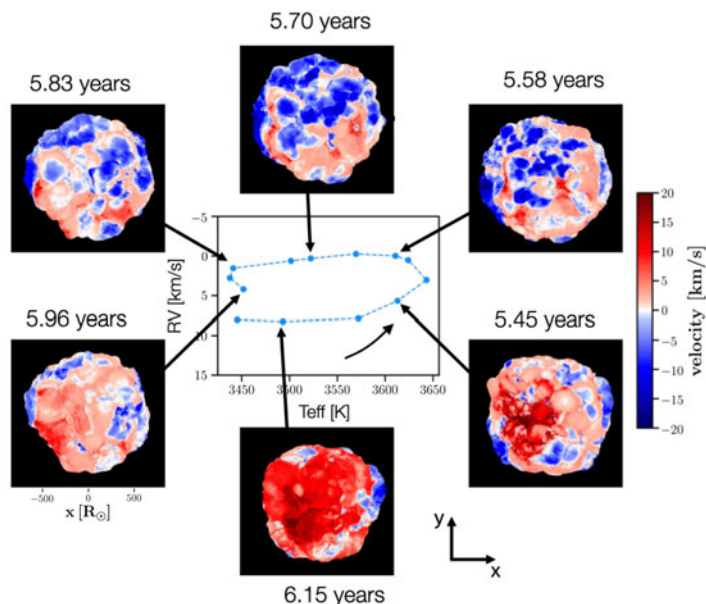


**Figure 7.** Velocity maps for different snapshots of a RSG simulation of Table 1 during a convection cycle (central part of the panel). The velocity is weighted with the contribution function, which is a useful diagnostics for studying spectral line formation in stellar atmospheres (e.g., Kravchenko et al. 2018). The red/blue colors correspond to inward/outward moving material, respectively. The central panel shows the behaviour of the radial velocity (RV). The arrow indicates the direction of the evolution along the hysteresis loop (Kravchenko et al. 2019, 2021).

Kravchenko et al. (2019) were able to interpret the long-term (almost 7 years of high-resolution spectra observed with the HERMES spectrograph) photometric variability of the RSG star  $\mu$  Cep. The authors denoted, in the observations, the presence of an hysteresis loop for convection. The hysteresis loop illustrates the convective turn-over of the material in the stellar atmosphere: first, the rising hot matter reaches upper atmospheric layers, then temperature drops as the matter moves horizontally and finally matter falls and cools down (Gray 2008). Kravchenko et al. (2019) showed that 3D RHD simulations explain this observed hysteresis behaviour and are useful to interpret time-dependent signatures, detectable in the observations, that rely on convection. As a matter of example, the velocity maps in Fig. 7 reveal upward and downward motions of matter extending over large portions of the stellar surface. The relative fraction of upward and downward motions is what distinguishes the upper from the lower part of the hysteresis loop (central panel of Fig. 7), its top part (zero velocity) being characterized by equal surfaces of rising and falling material. The bottom part of the hysteresis loop occurs, as expected, when the stellar surface is covered mostly by downfalling material.

Another example concerns the Great dimming episode of the RSG star Betelgeuse, when the brightness decreased dramatically to about 35% of its typical brightness in December 2019 (Guinan et al. 2020) before swiftly recovering over the next few months. Using the tomography and long-term HERMES data, Kravchenko et al. (2021) revealed the presence of two subsequent shocks in February 2018 and January 2019, the second one amplifying the effect of the first one. This produced a rapid expansion of a portion of the atmosphere of Betelgeuse and an outflow between October 2019 and February 2020. The final result was a sudden increase in molecular opacity in the cooler upper photosphere and, as a consequence, an unusual plumbing of the stellar brightness. This phenomenon has been described in the literature as ‘molecular plumes’ rising from the

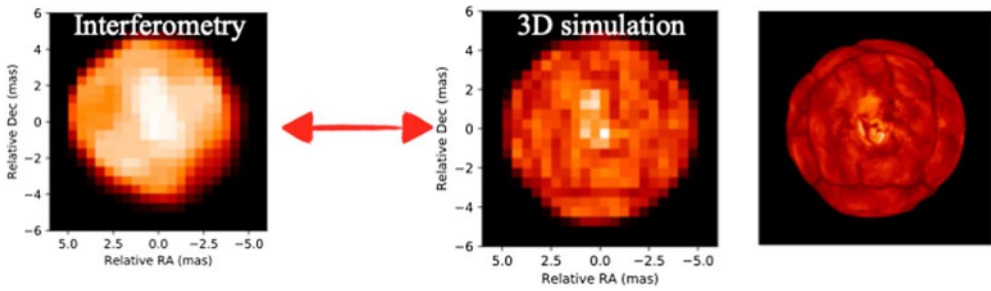


**Figure 8.** Representation of convective pattern size on a RSG star in observations and simulations. *Left panel:* Image of the stellar surface of the RSG CE Tau ( $M_{\star} \approx 15 M_{\odot}$ ,  $L_{\star} \approx 6.6 \times 10^4 L_{\odot}$ ,  $T_{\text{eff}} \approx 3820 \text{ K}$ ,  $R_{\star} \approx 587 R_{\odot}$ ,  $\log g \approx 0.05$ ) reconstructed from interferometric data collected with PIONIER@VLTI (Montargès et al. 2018). *Center and right panel:* Synthetic intensity map calculated from a 3D simulation ( $M_{\star} \approx 12 M_{\odot}$ ,  $L_{\star} \approx 8.9 \times 10^4 L_{\odot}$ ,  $T_{\text{eff}} \approx 3430 \text{ K}$ ,  $R_{\star} \approx 846 R_{\odot}$ ,  $\log g \approx -0.3$ , rightmost panel) and degraded to the observation spatial resolution (central panel).

photosphere of supergiants (Kervella et al. 2016) or molecular reservoirs (Harper et al. 2020). In the literature, there are also other explanations of this Betelgeuse’s dimming: Levesque & Massey 2020; Cotton et al. 2020; Safonov et al. 2020; Dupree et al. 2020; Dharmawardena et al. 2020; Montargès et al. 2021; Davies & Plez 2021.

#### 4.2. Spatially resolved surfaces: stellar surface details explained by simulations

Spatially resolved stellar surface observations, among which interferometry contributes substantially, are of great importance for evolved stars for two reasons: (i) they afford the direct detection and characterization of the convective pattern related to the surface dynamics, and (ii) they allow to determine the stellar parameters.

Two main observables are used in interferometry: the visibility and the closure phases. Visibilities measure the surface contrast of the source and are primarily used to determine fundamental stellar parameters and limb-darkening. Closure phases combine the phase information from three (or more) telescopes and provide direct information on the morphology of the source (Monnier 2003). The wise combination of both contributes to the image reconstruction of the observed targets. For a correct interpretation of the observations, it is necessary to simultaneously explain both observables with the same model as well as the intensity contrast and shape as a function of wavelengths. This is outlined in Fig. 8 where the reconstructed image (left panel) is compared to the synthetic image obtained from a 3D simulation (rightmost panel) convolved with the instrumental beam (central panel).

During the last decade, several observational works (Fig. 9) used 3D RHD simulations to explain the interferometric data of massive evolved stars. For instance, the first works concerned the RSG star Betelgeuse for which Chiavassa et al. (2009) and Chiavassa et al. (2010a) detected and measured the characteristic sizes of convective cells using measurements in the infrared and in the optical. Chiavassa et al. (2010b) and Chiavassa et al. (2021) reconstructed the images of another RSG, VX Sgr, with different instruments from the H to the N band to probe the presence of large convective cells on its surface. Montargès et al. (2014), Montargès et al. (2016), and Montargès et al. (2017) reported a series of reconstructed images, interpreted with 3D simulations, for several RSGs and different instruments (AMBER and PIONIER at VLTI).

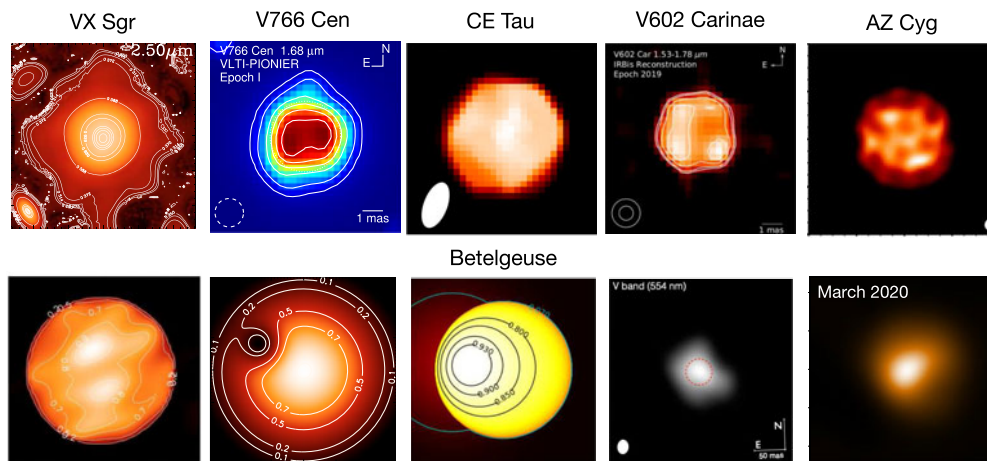


**Figure 9.** Few examples of images obtained from observations of different RSG stars. *Top row:* VX Sgr with AMBER@VLTI (Chiavassa et al. 2010b), V766 Cen with PIONIER@VLTI (Wittkowski et al. 2017), CE Tau with PIONIER@VLTI (Montargès et al. 2018), V602 Carinae with PIONIER@VLTI (Climent et al. 2020), AZ Cyg with MIRC@CHARA (Norris et al. 2021). *Bottom row:* Betelgeuse with IOTA and COAST interferometers (first two images, Chiavassa et al. 2010a), with PIONIER@VLTI (Montargès et al. 2016), with SPHERE (Kervella et al. 2016; Montargès et al. 2021).

However also the temporal evolution (at different wavelengths) is a key point in the understanding of stellar dynamics. For instance, Wittkowski et al. (2017), Montargès et al. (2018), Climent et al. (2020), Norris et al. (2021), and Montargès et al. (2021) showed the importance of temporal variability in the observations. To tackle all the different astrophysical problems related to evolved stars, recent and future interferometers have to challenge the combination of high spectral and spatial resolution as well as the time monitoring on relatively short timescales (weeks/month) of these objects (Chiavassa et al. 2011a; Montargès et al. 2021).

The direct measurement of stellar angular diameters has been the principal goal of most attempts with astronomical interferometers since the pioneering work of Michelson & Pease (1921). Nowadays with the advent of Gaia, for stars of known distance the angular diameter becomes of paramount importance to yield the stellar radius and eventually to the absolute magnitude. These quantities are essential links between the observed properties of stars and the results of theoretical calculations on stellar structure and evolution. Few survey works (Cruzalèbes et al. 2013; Arroyo-Torres et al. 2014, 2015; Wittkowski et al. 2017) characterized the fundamental parameters and atmospheric extensions of evolved stars in our neighbourhood using AMBER instrument (now decommissioned) at VLTI. In particular, the last two papers observed a linear correlation between the visibility ratios of observed RSGs and the luminosity and surface gravity, indicating an increasing atmospheric extension with increasing luminosity and decreasing surface gravity, indirectly supporting a mass-loss scenario of a radiatively driven extension caused by radiation pressure on Doppler-shifted molecular lines. These results are confirmed for AGB stars (Wittkowski et al. 2016) where the atmospheric extension is detected and explained by the RHD simulations for a sample of interferometric observations, supporting the mass-loss scenario of pulsation- and shock-induced dynamics that can levitate the molecular atmospheres of Mira/AGB variables to extensions that are consistent with observations.

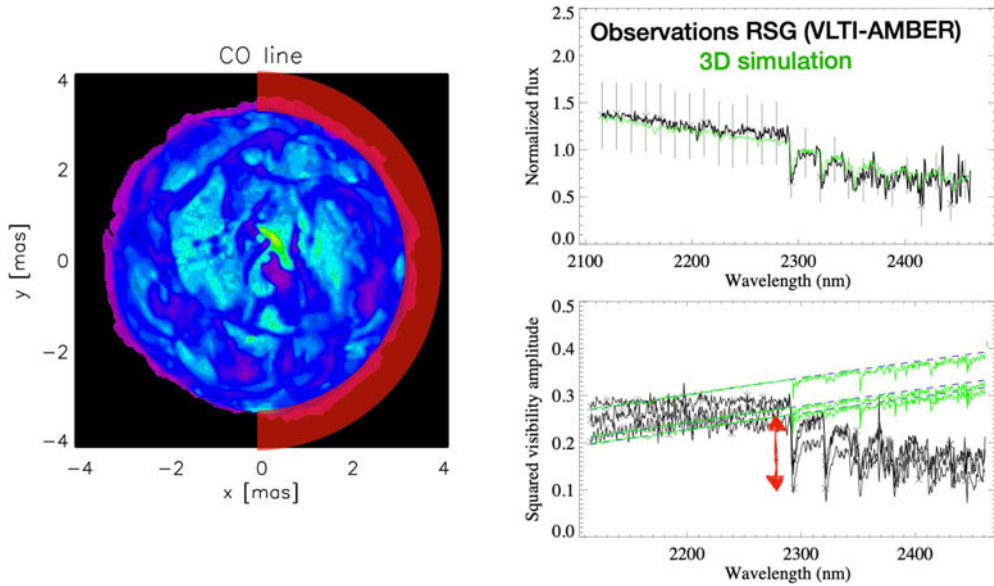


**Figure 10.** *Left panel:* Synthetic image in the Carbon Monoxide (CO) lines at about  $2.3\ \mu\text{m}$ . The semi-circle in red displays the expected atmospheric extension needed to explain the drop in the squared visibility (right panels). *Right panels:* Interferometric observations of red supergiants with AMBER (black) compared to 3D simulation predictions (green). While the flux adjustment (top panel) is in a good agreement, the synthetic visibilities cannot reproduce the observed atmospheric extension (bottom panel, red arrow). See [Arroyo-Torres et al. \(2015\)](#) for more details.

## 5. Improving 3D simulations: towards the solution of the mass-loss mechanism?

Recent advances in instrumental techniques in interferometry, imaging, and spectroscopy have achieved an astonishing level of accuracy. Despite the very satisfactory comparisons of the 3D simulations with observations, a number of studies have highlighted the current limitations of 3D simulations that need to be solved to provide a quantitative response to the problem of mass-loss in red supergiants. These four points are the cornerstone for future developments in the field and are listed below in order of importance.

- (1) *The radiative pressure.* A comparison of 3D simulations to interferometric observations with AMBER at VLTI have shown that the extension of the observed red supergiant atmospheres is not interpretable with current models ([Arroyo-Torres et al. 2015](#)). Figure 10 shows that while the synthetic flux is adequate to match the observed AMBER flux (top right panel), the squared visibility are completely off (bottom right panel). The interferometric visibilities are linked to the surface brightness contrast of the observed object. The observed visibility amplitudes show strong visibility drops in the molecular bands (emphasizing a major extension of the photosphere, red arrow in bottom right panel) that cannot be explained by the simulations. This is also visible in the synthetic intensity map (left panel) where the missing photospheric extension is highlighted in red. This finding was confirmed by the optical data obtained with SPHERE, where also here the extension of the 3D photosphere is too limited compared to the

observations (Kervella et al. 2016). The inclusion of radiative pressure in the simulations should help the gas to levitate in the outermost layers of the photosphere, where the molecular opacity is not negligible (e.g., TiO molecules) and explain (at least in part) the mechanism of mass loss: radiative pressure on molecules as suggested by Josselin & Plez (2007), based on an order of magnitude calculation by Gustafsson & Plez (1992).

- (2) *The magnetic field.* The presence of a magnetic field in stars is intimately linked to the convection across the stellar photosphere. A typically magnetic field results in the increase of atmospheric velocities and higher temperatures in the chromosphere. As a consequence, the overall structure of the stellar atmosphere is affected. In the case of evolved stars, local dynamos are expected to appear in correspondence to the large convective cells (Freytag et al. 2002). The introduction of a magnetic field into 3D simulations is under development and should produce large-scale local dynamos, that grow for decades and saturate with only moderate fluctuations. What has to be explored is the impact on the velocities in the lower photosphere. Here, the velocities should be reduced by the magnetic field. Meanwhile, in the outer layers (where the boundary conditions are crucial), the velocities should increase and sustain the stellar winds.
- (3) *The numerical resolution.* Resolving the turbulent character of an RSG photosphere is a complex task that has an impact on several aspects: model stratification, numerical viscosity, Doppler shift in the spectral lines. The spatial resolution of small-scale structures close to the grid box need large box sides (e.g.,  $1000^3$  or even larger depending on the spectral type) which is extremely computer-time intensive. Refining the computational box means resolving better the turbulent medium (Nordlund et al. 2009). The latter point is precisely what is missing in 3D RHD simulation. Figure 11 shows that the velocities in the simulations are at maximum 20-30 km/s (red curve), which is far too low to reach the escape velocity (light blue curve) even though the velocities are supersonic (the sound speed is plotted in violet). The under-estimation of the simulation's velocities has a direct consequence on the gas levitation by the vigorous convection in these stars. The current solution is to increase the number of points to at least  $1000^3$ .
- (4) *The stellar rotation.* Observations of Betelgeuse indicate that RSG stars may rotate: Uitenbroek et al. (1998) found with HST an angular rotational velocity between 2.0 and 2.5 km/s (i.e., a projected equatorial velocity of 5.0 km/s); Kervella et al. (2018) reported a projected equatorial velocity of about 5.47 km/s using ALMA. The observed rotational velocity is about six times lower than the turbulent velocity due to the convection-related surface structures, but it could also take part in the mass-loss mechanism. Freytag et al. (2017) described the effect of rotation on AGB simulations carried out with CO5BOLD and demonstrated that the temperature stratification shows hardly any effect, while the average density in the atmosphere increases with shorter rotation period. The authors insisted on the actual shortcomings in their simulations where the approximation of the smoothed stellar core plays a larger role than for purely convective flows that are not rotating. However, in the context of RSG stellar winds, it remains valuable to question how the angular momentum is advected in a very slowly rotating convective envelope and the role (if any) of the magnetic fields/convection coupling across the stellar photosphere and above.

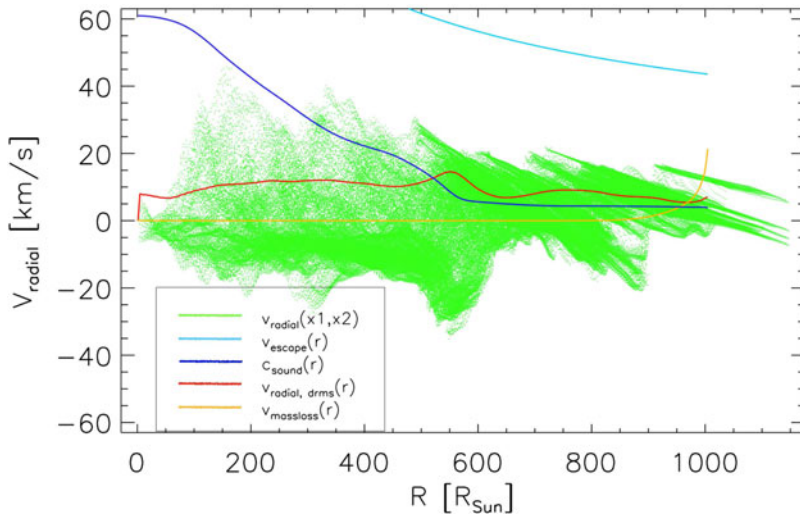


**Figure 11.** Scatter plot of the radial velocities (green points) for one particular snapshot of the 3D simulation of Table 1 and for all the grid points in the numerical box. The red line displays the velocities' spherical average. The violet line shows the sound speed. The light blue displays the escape velocities for a  $5 M_{\odot}$  star. The orange line is an example of 1D velocity derived from mass conservation for a mass-loss rate set to  $10^{-6} M_{\odot}/\text{yr}$ . The nominal radius of the simulation is  $582 R_{\odot}$  (Table 1).

## 6. Conclusions

We presented 3D radiation-hydrodynamics simulations for massive evolved RSG stars. These simulations are computed with the CO5BOLD code that takes into account the full convective envelope and are characterized by realistic input physics. The simulations reproduce the effects of convection and non-radial waves. RHD simulations predict photospheric structures with extremely inhomogeneous temperatures and densities. The rising material originates in the deep convective zone and develops as an atmospheric shock with supersonic velocities when it reaches the outer layers. Additionally, the important and natural temporal variability of the convective movements affects the stellar parameters and, more generally, all the observables of RSG stars. More details will appear in a future paper (Chiavassa & Kravchenko, 2022, Living Reviews in Computational Astrophysics).

The stellar variability, heterogeneity, and dynamics demonstrated by 3D RHD simulations of RSGs may have an impact on the environment of core-collapse supernovae (Giacinti et al. 2019); on the quantitative studies of metallicity in our Galaxy (Levesque 2018) and in nearby galaxies (Davies et al. 2017); and on the mass-loss mechanism and thus in the physics implemented in stellar evolution codes (Meynet et al. 2015).

These stars are among the largest stars in the Universe and their luminosities place them among the brightest stars, visible to very long distances. RSGs are major cosmic engines with strong stellar winds whose origin is still under debate. Ongoing and future developments of 3D RHD simulations will help to lead towards the solution of the mass-loss problem.

## References

- Alvarez, R., Jorissen, A., Plez, B., et al. 2000, *A&A*, 362, 655
- Alvarez, R., Jorissen, A., Plez, B., et al. 2001, *A&A*, 379, 305
- Alvarez, R., Jorissen, A., Plez, B., et al. 2001, *A&A*, 379, 288
- Arroyo-Torres, B., Martí-Vidal, I., Marcaide, J. M., et al. 2014, *A&A*, 566

- Arroyo-Torres, B., Wittkowski, M., Chiavassa, A., et al. 2015, *A&A*, 575, A50
- Asplund, M., Grevesse, N., Sauval, A. J., et al. 2009, *ARAA*, 47, 481
- Aurière, M., Donati, J.-F., Konstantinova-Antova, R., et al. 2010, *A&A*, 516, L2
- Cannon, E., Montargès, M., de Koter, A., et al. 2021, *MNRAS*, 502, 369
- Chiavassa, A., Plez, B., Josselin, E., et al. 2009, *A&A*, 506, 1351
- Chiavassa, A., Haubois, X., Young, J. S., et al. 2010, *A&A*, 515, A12
- Chiavassa, A., Lacour, S., Millour, F., et al. 2010, *A&A*, 511, A51
- Chiavassa, A., Pasquato, E., Jorissen, A., et al. 2011a, *A&A*, 528, A120
- Chiavassa, A., Freytag, B., Masseron, T., et al. 2011b, *A&A*, 535, A22
- Chiavassa, A. & Freytag, B. 2015, Why Galaxies Care about AGB Stars III: A Closer Look in Space and Time, 497, 11
- Chiavassa, A., Kravchenko, K., Millour, F., et al. 2020, *A&A*, 640, A23
- Chiavassa, A., Kravchenko, K., Montargès, M., et al. 2021, *A&A* in press, arXiv:2112.10695
- Clement, J. B., Wittkowski, M., Chiavassa, A., et al. 2020, *A&A*, 635, A160
- Cotton, D. V., Bailey, J., De Horta, A. Y., et al. 2020, Research Notes of the American Astronomical Society, 4, 39
- Cranmer, S. R. & Saar, S. H. 2011, *ApJ*, 741, 54
- Cruzalèbes, P., Jorissen, A., Rabbia, Y., et al. 2013, *MNRAS*, 434, 437
- Davies, B., Kudritzki, R.-P., Lardo, C., et al. 2017, *ApJ*, 847, 112
- Davies, B. & Plez, B. 2021, *MNRAS*, 508, 5757
- De Beck, E., Decin, L., de Koter, A., et al. 2010, *A&A*, 523, A18
- Decin, L., Montargès, M., Richards, A. M. S., et al. 2020, *Science*, 369, 1497
- Decin, L. 2021, *ARAA*, 59, 337
- Dharmawardena, T. E., Mairs, S., Scicluna, P., et al. 2020, *ApJ*, 897, L9
- Dupree, A. K., Strassmeier, K. G., Matthews, L. D., et al. 2020, *ApJ*, 899, 68
- Freytag, B., Steffen, M., & Dorch, B. 2002, *Astronomische Nachrichten*, 323, 213
- Freytag, B., Steffen, M., Ludwig, H.-G., et al. 2012, *Journal of Computational Physics*, 231, 919
- Freytag, B., Liljegren, S., & Höfner, S. 2017, *A&A*, 600, A137
- Giacinti, G., Dwarkadas, V., Marcowith, A., et al. 2019, 36th International Cosmic Ray Conference (ICRC2019), 36, 74
- Gray, D. F. 2008, *ApJ*, 135, 1450
- Guinan, E., Wasatonic, R., Calderwood, T., et al. 2020, The Astronomer's Telegram, 13512
- Gustafsson, B. & Plez, B. 1992, Instabilities in Evolved Super- and Hypergiants, 86
- Gustafsson, B., Edvardsson, B., Eriksson, K., et al. 2008, *A&A*, 486, 951
- Harper, G. M., Guinan, E. F., Wasatonic, R., et al. 2020, *ApJ*, 905, 34
- Haubois, X., Perrin, G., Lacour, S., et al. 2009, *A&A*, 508, 923
- Höfner, S. & Freytag, B. 2019, *A&A*, 623, A158
- Höfner, S. & Olofsson, H. 2018, *ARAA*, 26, 1
- Josselin, E. & Plez, B. 2007, *A&A*, 469, 671
- Kervella, P., Lagadec, E., Montargès, M., et al. 2016, *A&A*, 585, A28
- Kervella, P., Decin, L., Richards, A. M. S., et al. 2018, *textitA&A*, 609, A67
- Kiss, L. L., Szabó, G. M., & Bedding, T. R. 2006, *MNRAS*, 372, 1721
- Kravchenko, K., Van Eck, S., Chiavassa, A., et al. 2018, *A&A*, 610, A29
- Kravchenko, K., Chiavassa, A., Van Eck, S., et al. 2019, *A&A*, 632, A28
- Kravchenko, K., Jorissen, A., Van Eck, S., et al. 2021, *A&A*, 650, L17
- Langer, N. 2012, *ARAA*, 50, 107
- Lebzelter, T., Trabucchi, M., Mowlavi, N., et al. 2019, *A&A*, 631, A24
- Levesque, E. M., Massey, P., Olsen, K. A. G., et al. 2005, *ApJ*, 628, 973
- Levesque, E. M. 2018, *ApJ*, 867, 155
- Levesque, E. M. & Massey, P. 2020, *ApJ*, 891, L37
- Liljegren, S., Höfner, S., Freytag, B., et al. 2018, *A&A*, 619, A47
- Mathias, P., Aurière, M., López Ariste, A., et al. 2018, *A&A*, 615, A116
- Meynet, G., Chomienné, V., Ekström, S., et al. 2015, *A&A*, 575, A60

- Michelson, A. A. & Pease, F. G. 1921, *ApJ*, 53, 249. doi:10.1086/142603
- Monnier, J. D. 2003, *Reports on Progress in Physics*, 66, 789
- Montargès, M., Kervella, P., Perrin, G., et al. 2014, *A&A*, 572, A17
- Montargès, M., Kervella, P., Perrin, G., et al. 2016, *A&A*, 588, A130
- Montargès, M., Chiavassa, A., Kervella, P., et al. 2017, *A&A*, 605, A108
- Montargès, M., Norris, R., Chiavassa, A., et al. 2018, *A&A*, 614, A12
- Montargès, M., Cannon, E., Lagadec, E., et al. 2021, *Nature*, 594, 365
- Nordlund, Å., Stein, R. F., & Asplund, M. 2009, *Living Reviews in Solar Physics*, 6, 2
- Norris, R. P., Baron, F. R., Monnier, J. D., et al. 2021, *ApJ*, 919, 124
- Ohnaka, K., Weigelt, G., & Hofmann, K.-H. 2017, *Nature*, 548, 310
- Safonov, B., Dodin, A., Burlak, M., et al. 2020, arXiv:2005.05215
- Uitenbroek, H., Dupree, A. K., & Gilliland, R. L. 1998, *ApJ*, 116, 2501
- Wittkowski, M., Chiavassa, A., Freytag, B., et al. 2016, *A&A*, 587, A12
- Wittkowski, M., Arroyo-Torres, B., Marcaide, J. M., et al. 2017, *A&A*, 597, A9
- Wittkowski, M., Abellán, F. J., Arroyo-Torres, B., et al. 2017, *A&A*, 606, L1

## Discussion

ORSOLA DE MARCO: There is a large literature on stabilising large stars like RSG and AGB for common envelope simulations. I do not understand how you overcome some numerical challenges in particular when computing the luminosity of the star. What do you do when you set up your star?

ANDREA CHIAVASSA: In a cartesian equidistant box, the initial model is produced starting from a sphere in hydrostatic equilibrium with a weak velocity field inherited from a previous model with different stellar parameters. The input luminosity enters into few central grid cells of the box and the envelope stellar mass in the equation for the gravitational potential. After some time, the limb-darkened surface without any convective signature appears but with some regular patterns due to the numerical grid. After several years of stellar time, a regular pattern of small-scale convection cells develops and, after cells merge the average structures, it becomes big and the regularity (due to the Cartesian grid) is lost. The intensity contrast grows with time.

ILEYK EL MELLAH: Did you try to inject any molecular network? Do you have an idea of the distribution of abundances of molecular species as a function of distance? Is this coherent with the olivine detection you see in VX Sgr?

ANDREA CHIAVASSA: No, we did not try so far to include any molecular network dependence. The approach presented is related to a tentative model fitting with RADMC3D code and there is not, so far, a link with the expected abundances of molecules in the extended photosphere. However, this is something we have in mind to do in the future.

RAGHVENDRA SAHAI: In your very sophisticated simulations, the word chromosphere did not come out. Do you produce something like a chromosphere in these models? Is there a reasonable amount of ionised gas around these stars?

ANDREA CHIAVASSA: Indeed, in our actual simulations, the temperature and density drops go farther from the star and thus we can say that the chromosphere is not included so far.

LEEN DECIN: The formation of carbon Monoxide is calculated using a thermal equilibrium scheme? and so what is the abundances used?

ANDREA CHIAVASSA: Yes, it was at thermal equilibrium with solar metallicity. Maybe I was a bit quick on this point during the talk. The spectro-interferometric observations I showed concerned the flux and the visibility curves. While the synthetic flux had a good agreement with observations, the visibility (ie, the spatially resolved intensity brightness) was completely off. This means that we cannot resolve the extension of the atmosphere of those stars while we actually reproduce the integrated flux of the object.

LEEN DECIN: Is it enough to approximate the contribution to the photospheric flux using two different hydrostatic MARCS models? In the case of Betelgeuse?

ANDREA CHIAVASSA: In the paper we did with Ben Davies in 2013, we used two MARCS components to mimic the surface brightness of the 3D simulated. However, I think that we would need many more 1D structures for this purpose.

BEN DAVIES: Comment. We recently added a Betelgeuse wind to the MARCS structure, including temperature inversion in the upper wind and we obtain a very good fit of the entire SED.